LJMU Research Online

Zhang, G, Lee, C, Harvey, D and Ma, H

 Development of C-Line plot technique for the characterization of edge effects in acoustic imaging: A case study using flip chip package geometry

http://researchonline.ljmu.ac.uk/id/eprint/1980/

Article

Development of C-Line plot technique for characterization of edge effects in acoustic imaging: A case study using flip chip package geometry

Chean Shen Lee[1], Guang-Ming Zhang[1], David M Harvey[1], Hong-Wei Ma[2]*

[1]General Engineering Research Institute, Liverpool John Moores University
James Parson Building, Byrom Street, L3 3AF, United Kingdom

[2]School of Mechanical Engineering, Xi'an University of Science and Technology, Xi'an, 710054, China

[*] Corresponding author. Tel: +44-1512312113; E-mail: g.zhang@ljmu.ac.uk.

Abstract

Edge effect is a common phenomenon observed in Acoustic micro imaging of microelectronic packages. In this paper, using flip chip package geometry as a test vehicle, finite element modelling is carried out to study the fundamental mechanism of the edge effect phenomenon. C-line plot technique is developed for characterisation of edge effects in acoustic C-scan images, in particular solder joint C-scan images. Simulated results are compared to experimental results. Results reveal that edge effect generation is mainly attributed to the under-bump-metallisation structure. In addition, through analysis of the C-Line profile of edge effects, the impact of the transducer focal point and the spot size on the edge effect is investigated. Results show that slight off-focus can reduce the severity of the edge effect in which image sharpness is a trade-off.

Keywords: Edge effect; Flip chip packages; Acoustic micro imaging; Finite element modelling; Under-bump-metallisation

1. Introduction

Acoustic Micro Imaging (AMI) is a well-established method for non-destructive evaluation (NDE) of microelectronic packages. AMI has strong penetration capabilities and is very effective at detecting discontinuities within materials and interconnects [1-3]. In practical AMI systems, the sample is normally submerged in water to reduce acoustic impedance mismatch. A focused ultrasonic transducer sends pulses into and receives reflected echoes from features within the sample alternatively. The transducer characteristics such as the transducer frequency, focal length, diameter of the acoustic lens, and spot size define the imaging resolution and the complex wave propagation in the sample. Thus, a suitable transducer has to be chosen according to the test sample. Based on the depths of the reflecting features in the sample, a gate corresponding to a time window is normally used to select a specific depth or interface to view. A mechanical scanner moves the transducer in a zig-zag way over the sample, producing a C-scan (interface scan) image. At each x-y position the peak intensity value of the received echo signal within the gate is displayed in the C-scan image. Fig. 1 shows a C-scan image of the silicon die-solder bump interface obtained from the inspection of a flip-chip package soldered on a PCB board [3]. The flip chip packages contained 109 solder joints positioned at the periphery of the package. The silicon die size of the flip chip is 3948 µm × 8898 µm and the die thickness is 725 µm. The solder bump diameter is 140 µm with a height of 125 µm. The under-bump-metallisation (UBM) composition is Al/NiV/Cu thin film metal stack with a pad size of 90 µm × 90 µm.

The Edge Effect Phenomenon (EEP) is a common phenomenon observed in Acoustic micro imaging of microelectronic packages. The phenomenon is usually observed at the edge or perimeter of the die or package as well as on the outer radius of solder balls as shown in Fig. 1. Especially for solder bumps, the phenomena manifests itself as a dark ring around the solder bump as shown in Fig. 2, indicating that most if not all of the incident acoustic energy has been angularly-reflected by the curvature of the solder ball geometry. The dark annular region can obscure the detection of defects such as cracks and voids inside the solder bump [2-4]. Consequently, the interpretation of C-scan images and defect detection of solder joints becomes difficult.
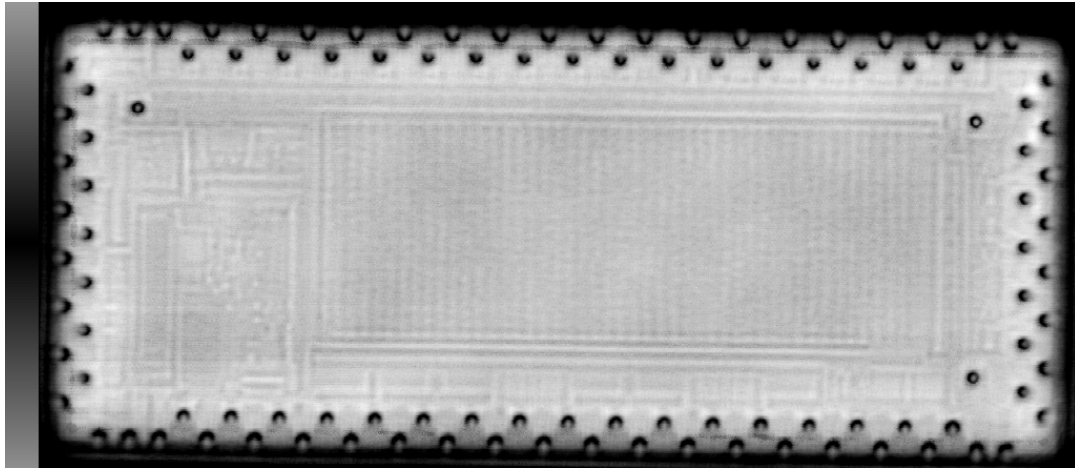
Fig. 1. A plan of a c-scan image of flip chip package soldered on a PCB board using a 230 MHz transducer with a spot size of 16 µm and focal depth of 186 µm.
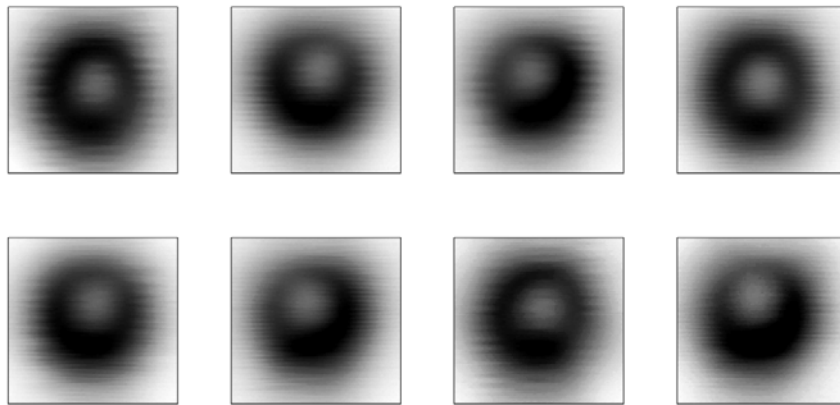

Fig. 2. Typical C-scan images of solder joints extracted from Fig. 1.

It is widely accepted that edge effects occur when the acoustic wave is diffracted or angularly-reflected either by the edge geometry or refracted when the ultrasonic echo is propagating through various materials [1]. The physical explanation for the generation of edge effects is still not clear. Moreover, the acoustic pulse propagation mechanism within the solid specimen cannot currently be measured directly. In this paper, finite element modelling is proposed to investigate acoustic wave propagating in microelectronic structures and to study the fundamental mechanism of the edge effect phenomenon. A novel C-Line plot technique is proposed to characterize the edge effects of acoustic C-scan images, particularly in solder joint C-scan images. The relationship between the edge effect and the solder bump condition can be used to develop quantitative defect detection algorithms in the future.

2. Finite element modelling and acoustic simulation

In order to study the fundamental mechanism of the edge effect phenomenon, finite element modelling based on the flip chip package geometry and a virtual transducer is firstly carried out in Section 2.1. Then acoustic simulation of the acoustic wave propagation in the flip chip package is studied in Section 2.2 and B-scan images are obtained through the acoustic simulation.

2.1 Finite element modelling
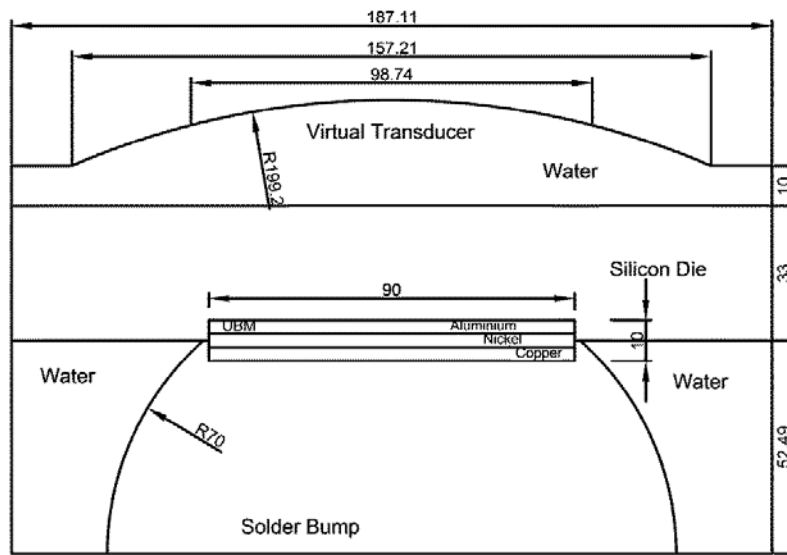
Fig.3. The geometrical model for acoustic simulation (units in µm).

A geometrical model shown in Fig. 3 was built on the basis of the physical flip chip test sample inspected by a scanning acoustic microscope as used in our practical experiments. Three finite element models were built on the basis of the geometrical model with the model variations listed in Table 1 and the global model parameters listed in Table 2.

Table 1: Three finite element models.

Model Name	Silica Connection	Additional Parameters
Model A1	UBM	Focal point at centre of UBM sandwich
Model A2	UBM	Focal point in solder bump 3µm below UBM
Model B	NO UBM	Focal point at centre of UBM sandwich

Table 2: Model parameters.

Structure	Parameters
Solder Bump Diameter	140 µm
Solder Material	Tin-Lead (60:40)
UBM Composition	Al, NiV, Cu; Ratio 1:1:1
UBM Thickness	10 µm
Silicon Die Thickness	33 µm

A Virtual Transducer (VT) is modelled against the physical 230 MHz focused transducer used in our experiments. The 230 MHz Sonoscan transducer has a lens diameter of 4750 µm, a focal length of 9500 µm in water, a spot size of 16 µm, and a focal depth (depth of focus or depth of field) of 186 µm in water. The VT derived from the physical transducer includes two key parameters: the VT curvature and the arc length. The arc length C_0 as shown in Fig. 4 defines the active region of the VT geometry which is coupled with pressure loads and data points to transmit and receive acoustic signals. The arc length is related to the chord length of the circle given as:

$$Chord = 2R \sin(\arcsin \frac{C_0}{2R_0}), \quad (1)$$
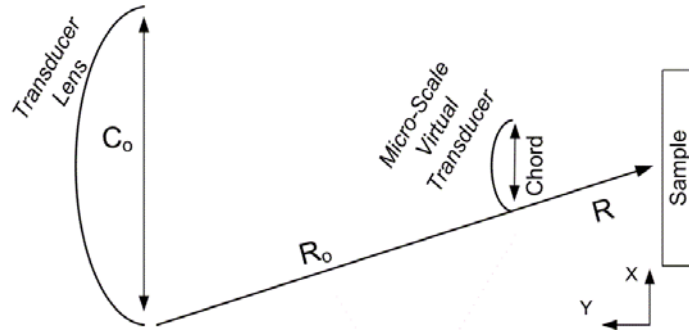
Fig. 4. The virtual transducer derived from the physical transducer to reduce computational load.

where R is the radius of the VT curve, C_0 and R_0 are the lens diameter and focal length of the physical transducer respectively.

An ultrasonic signal is usually a broadband pulse modulated at the centre frequency of the transducer, and is usually modelled as a Gabor function as follows:

$$f(t) = A \cdot \exp\left(-\frac{\pi(t-u)^2}{\sigma^2}\right) \cdot \cos(\omega(t-u)), \quad (2)$$

where A is the reference amplitude, ω is the frequency modulation and u its translation and σ controls the envelope of the Gaussian function. Our previous research showed that for the 230 MHz focused transducer, the approximate error (the root-mean squared error) using the Gabor model is smaller than 1.12% [5]. Therefore, the input displacement loads applied to the virtual transducer were modulated using the Gabor function in Eq. (2). The parameters in Eq. (2) were obtained by approximating a reference ultrasonic echo using the Gabor model as described in [5]. The parameters specifically for the physical 230 MHz transducer are ω = 0.4396 and σ = 19.1943. The displacement loads are then vectored in a tangent to the virtual transducer curve. The length of excitation loads along the virtual transducer is depended on the chord as shown in Fig. 4 and Eq. (1). In this paper, the chord has a length of 98.74 µm and a curvature radius of 199.2 µm as shown in Fig. 3. The distance from the VT to the test sample is 10 µm. The VT construction prevents the need to simulate large portions of fluid and structural domain and speeds up the simulation enormously, otherwise the simulation is impractical to be implemented in a PC.

The characteristics of the designed virtual transducer were verified by investigating its beam profile in water. Our numerical verification showed the VT has an operating frequency of 230 MHz, a bandwidth of 100 MHz, a spot size of 15 µm and a focal depth of 192 µm in water, which are very close to the characteristics of the physical transducer. The verification details can be found in [6, 7].

Since the physical transducer has a lens diameter of 4750 µm and a focal length of 9500 µm in water, the transducer will have to be placed around 6000 µm above the flip chip package in order to focus through the silicon die with a thickness of 725 µm. If we place the VT 10 µm above the test sample as in Fig. 3, the virtual transducer will have a diameter of over 1400 µm according to Fig. 4 and Eq. (2). Such a scale will present a problem for a high frequency acoustic simulation since the element density is tied to the wavelength. Therefore, in the finite element modelling, the thickness of the silicon die is reduced to 33 µm, and the processing time of the solution in our PC (Intel i7 cpu and 16 gb memory) is about **100 hours**. The solder joints are particularly vulnerable to crack initiations at the die-solder interconnect [8], resulting in great interest of the reliability of this region. The silicon die thickness of 33 µm was determined by calibrating the focal point of the virtual transducer into the middle of the UBM structure to achieve an optimal focus at the UBM structure. The calibration is based on the refractive principle of the wave travelling from the medium of water into the silicon die [6, 7].

Two-dimensional finite element modelling is carried out in this paper since using 3D models are too computationally intensive, and impractical to be implemented in a PC; the solder bump is symmetrical; the physical AMI system uses line scanning, and we only need to replicate individual line scans to produce comparable results. Three finite element models are studied in this paper as shown in Table 1. The models A1 and B used a virtual transducer radius of 199.2 µm, which focuses the acoustic energy at the centre of the UBM sandwich. However, there is no UBM structure in the model B, and the solder bump is directly connected to the silicon die. The model A2 uses a VT with the radius of 222.8 µm which places the focal point within the solder bump at around 3 µm below the UBM sandwich. This will produce the data for the effects of off-focusing which is used in practise to reduce edge effect severity. The focal point was measured in silicon because the exact focal point with a UBM present is difficult to ascertain due to the complex propagation mode in the multi layered structure. The model specifications are summarized in Table.

The models A1 and A2 are the 2-D cross section of a flip chip solder bump construction with the UBM composition from [9]. The numerical models are constructed in ANSYS APDL as shown in Fig. 5. The VT curvature difference in the models A1 and A2 were indiscernible so that Fig. 5 can represent both models. The right side of the model is elongated to accommodate the movement of the solder bump. This replicates the transducer mechanical scanning by redrawing the solder bump structure at 1 µm offset on the x-axis for each iteration. Central regions like A16, A13, A12, A18, A5, A3 and the UBM sandwich were defined by a high mesh density of 15 elements per wavelength (EPW). Our verification in [7] shows that 15 EPW is the optimal trade-off between the simulation accuracy and computation load. The surrounding buffer regions had a low mesh density of 5 to 10 EPW depending on their proximity from the high mesh density region in order to reduce the computation load. The 'frames' around certain geometries are there to accommodate the mismatch of the mesh density which minimize element distortions.
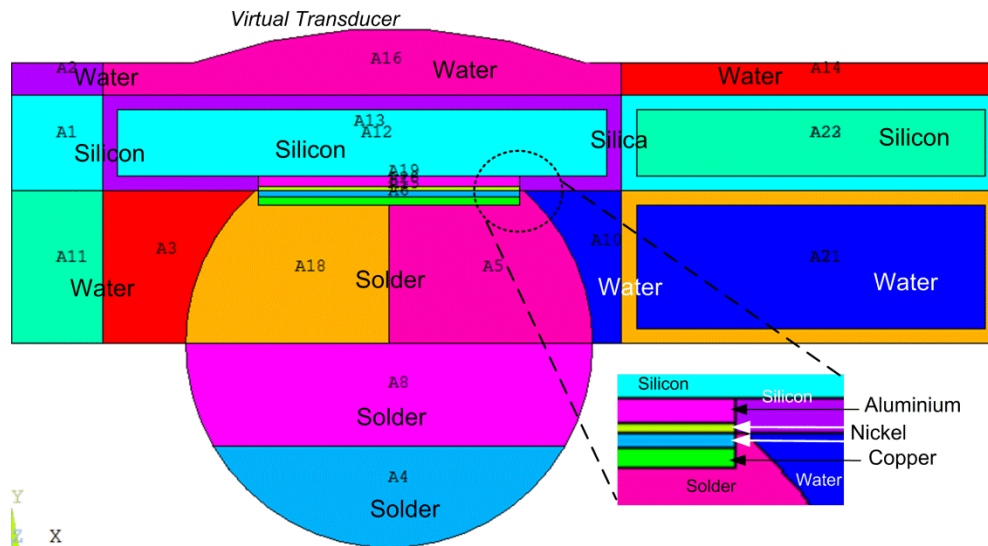
Fig. 5. The models A1and A2.

The model B as shown in Fig. 6 is constructed by directly removing the UBM and allowing the solder to connect directly to the silicon die. This will provide an acoustic response where the additional impedance offered by an UBM sandwich was non-existent. Comparisons between the models A1 and B will differentiate the severity of the edge effect caused by the UBM edge and the solder bump edge respectively. The model B shares the same focal length as the model A1 which will focus the pulse at the silicon die - solder bump interface.
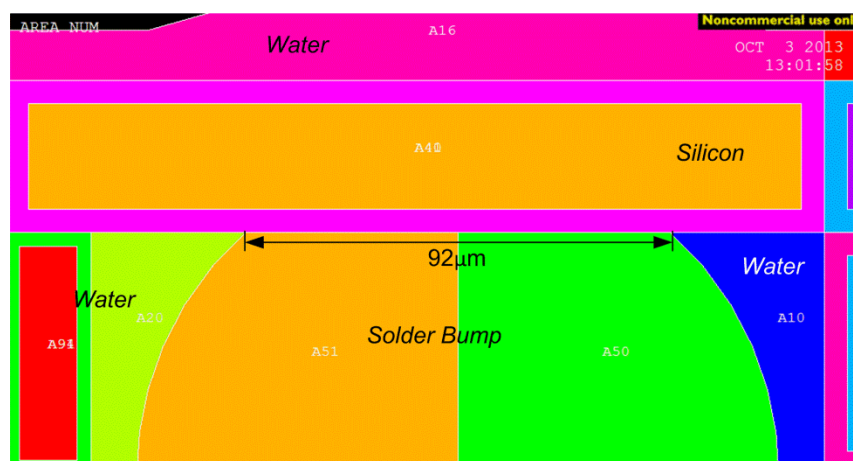

Fig. 6. The model B.
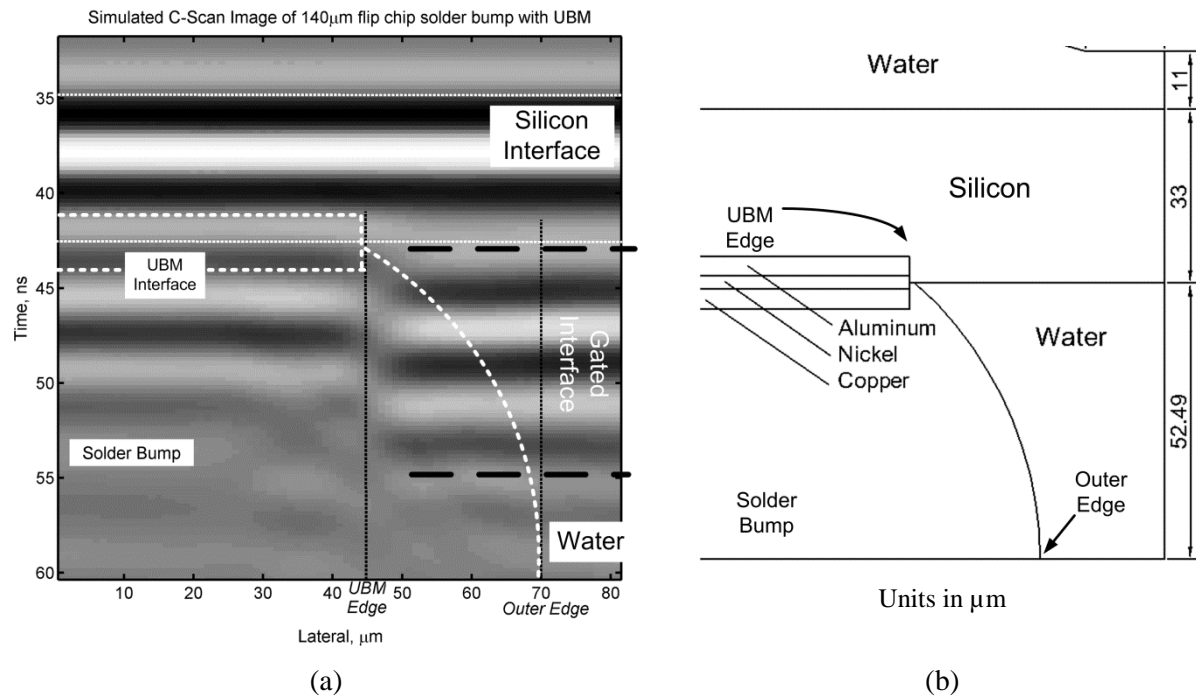
2.2 Acoustic simulation

Fig. 7. (a) Simulated B-scan image and (b) comparison with model

In order to replicate the scanning mechanism of the physical transducer, the solder bump is scanned horizontally at 1 µm interval. At each of these iterations, the model is redrawn and resolved. An A-scan signal is produced at each simulation *iteration*. The resultant A-scans are assembled to create a B-scan image as shown in Fig. 7(a). The B-scan is a cross-sectional image of the flip chip or a direct acoustic interpretation of the finite element model. In the B-scan, the y-axis represents the acoustic time-of-flight and the x-axis is the iteration which represents the transducer scanning position, giving the lateral dimension of the model. The actual model is presented in Fig. 7(b) for the purpose of reference. From the B-scan, the depth of the reflection interface and its approximate linear dimensions in the scan direction can be determined. The interface annotations shown in Fig. 7(a) can refer to Fig. 7(b). Note that, since the solder bump structure is symmetrical, only half of the model is scanned. Thus, the position of 0 µm on the lateral axis in Fig. 7(a) represents that the transducer is located on the centre axis of the solder bump. This reduces the required number of iterations by half from 160 to 80.

3. C-Line plots from simulated and measured data

To obtain the C-Line plot from the B-scan, the desired interface must be gated. Since the silicon die-solder bump interface is mainly concerned in reliability testing of flip chip packages, the gate is selected from rows 43 ns to 55 ns as shown in Fig. 7(a). The maximum amplitude value is then calculated from the gated signal. The gap in the bands shown around the "UBM Edge" lines in Fig. 7(a) is caused by loss of acoustic energy and manifests itself as a dip in the image intensity around the resultant C-Line plot of Fig. 8(a). As the transducer moves towards the edge of the solder bump, the image intensity increases due to high reflection from the silicon die-water interface. Overall, the decreased intensity between the strong reflections creates a "valley" profile which characterizes the edge effect phenomena as highlighted in Fig. 8(a). If required, the C-Line data can be mapped around a central axis to create a simulated C-scan image as shown in Fig. 8(b).

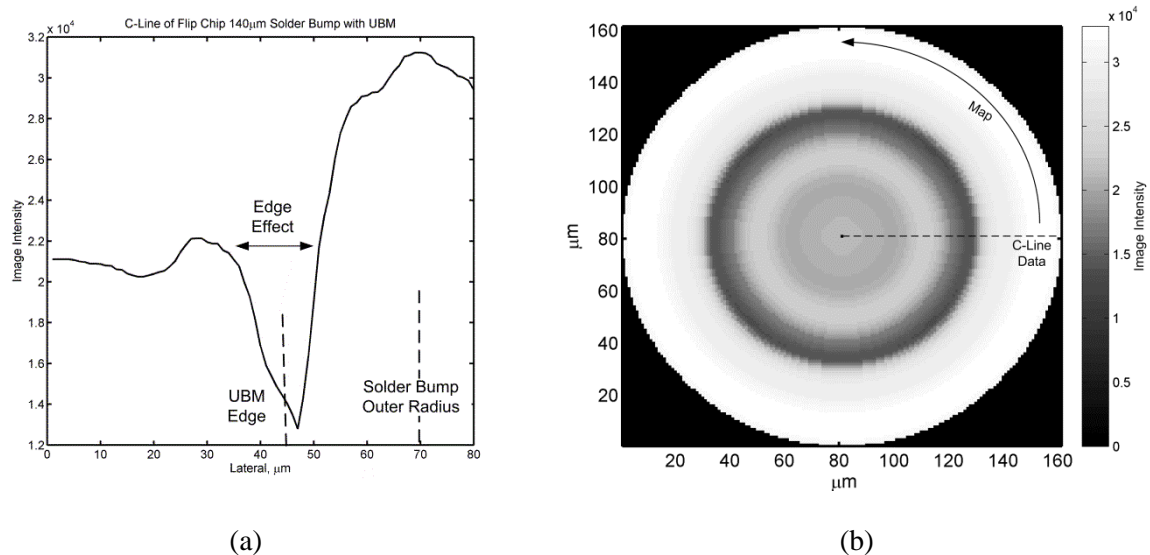(a)   (b)

Fig. 8. (a) A C-Line plot obtained from the simulated B-scan image in Fig. 7(a); (b) C-scan image created from the C-Line plot of Fig. 8(a).

Fig. 9(a) shows a silicon die-solder bump C-scan image measured using a 230 MHz transducer with a scanning resolution of 1 μm per pixel. The test sample is the same flip chip shown in Fig. 1. C-Line plots are cross-sectional plots from the measured C-scan image. The image intensity along the X-axis and Y-axis in Fig. 9(a) are extracted to create the C-Line plots shown in Fig. 9(b).
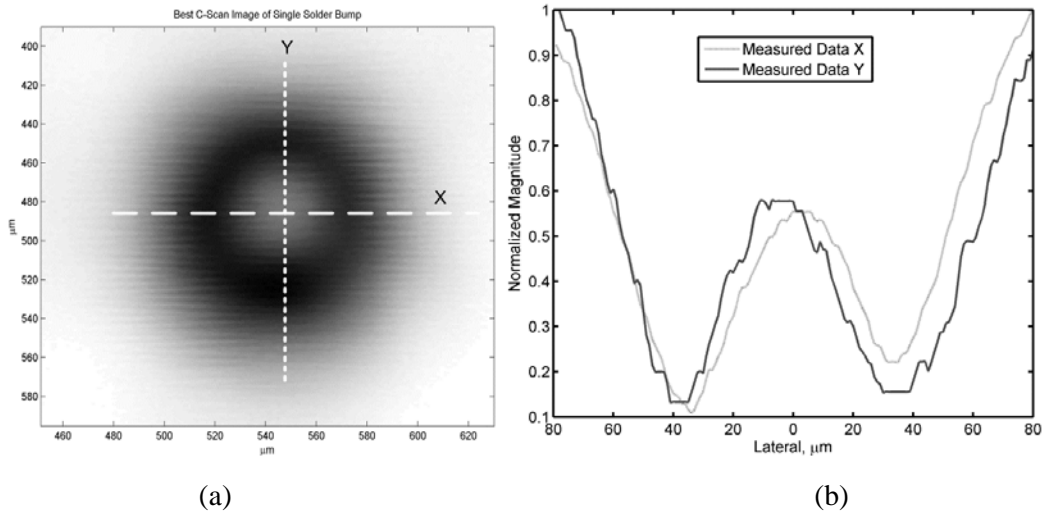
Fig. 9. (a) A measured C-scan image and (b) two resultant C-Line plots.

4. Characterisation of edge effect using c-line plot

In Section 4.1, the C-line plot technique developed in Section 3 is used to characterise the edge effects in solder joint C-scan images. Simulated results are presented and compared to experimental results. In Section 4.2, the impact of the transducer focal point and the spot size on the edge effect is investigated through analysis of the C-Line profile of edge effects.

4.1 Characterisation of edge effect

Fig. 10 shows a comparison between two C-Line plots obtained from experimental measurements against the simulated C-Line plot using the model A1. Annotations are introduced to provide consistent names of various characteristics of the C-Line to assist discussion and quantification. The edge effects are characterized by a drop in acoustic energy received by the transducer as it scans close to the UBM edge. When the transducer scans past the edge, the strong impedance mismatch between the silicon die and water produces a strong echo. This translates into a "W" shape profile on the C-Line.

At the centre of the solder bump, the C-Line plot has a relatively flat profile. This region has been named the *cap* as seen in Fig. 10. The initial atrophy of the acoustic magnitude was named the *sink transition*. This was followed by the *dip* which is the minimum caused by the edge effect. As the echo increases in magnitude towards the outer solder bump radius, this gradient was called the *rise transition*. For quantitative evaluation, the *sink point and rise point*, which were defined by the centre of their respective transition gradients, were introduced to measure the *dip width* that is the lateral distance between these two points.
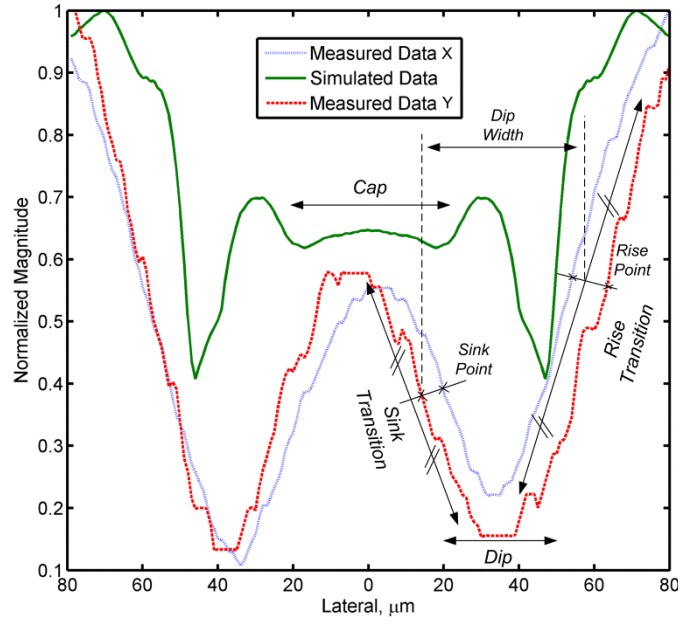
Fig. 10. Comparison of measured and simulated C-Line with annotations

Observations from Fig. 10 show that the edge effect *dip* is significantly deeper for the measured image. This is likely due to the thinner silicon die used in the numerical models. This effect is consistent to die back thinning which is shown to significantly reduce the edge effect generation as shown in [10]. In experimental measurements, slight adjustments in the focal point can have drastic effects on the resultant image. This is apparent in the simulated data where the models A1 and A2 have slight differences in their focal points. Fig. 11 shows considerable differences in the edge effect profile where the model A2 has a deeper *dip* and the edge effect *dip width* is 8 µm which is 4 µm narrower than the model A1 with a *dip width* of 12 µm. This means that slight off-focusing can help alleviate the edge effect in acoustic micro imaging of microelectronic packages. However, the C-Line of the model A1 shows more features are resolved as the acoustic energy is sharply focused at the UBM. In contrast, The model A2 has less information in its C-Line profile. For the model A2, the focal point is 3 µm off beneath the UBM structure, this means the acoustic energy reflected off the UBM structure was not converged into its minimum size. This is equivalent to imaging with a larger acoustic spot size.
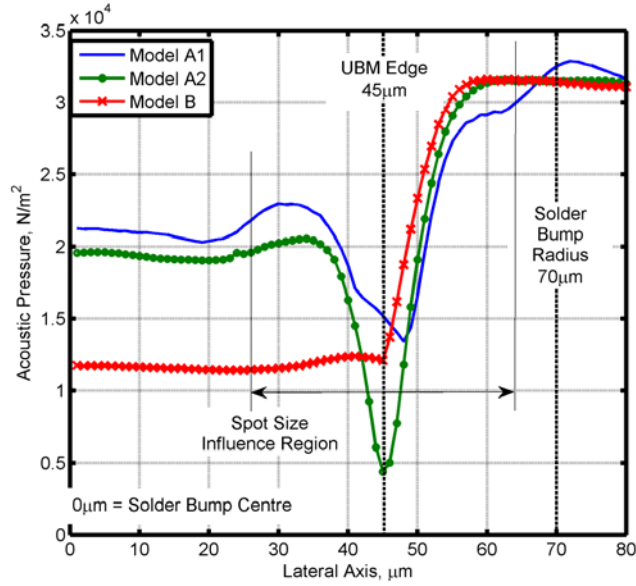
Fig. 11. C-Line profile comparison between the models A1, A2 and B for half a solder bump.

The C-Line for the model B (which does not have an UBM), does not have a noticeable *sink transition*. The characteristic "V" shape profile is missing. From Fig. 11, it can be seen that the edge effect is mainly attributed to the multilayered UBM structure. It is also observed that without the UBM structure, more acoustic energy penetrates into the solder bump. It is worth noting that the *rise transition* of the model B is actually akin to a "step increase" compared to a more sporadic transition of the models A1 and A2. Hence, the model B can be considered to have limited edge effects. However, the model B is not realistic, since there will always be a UBM.

4.2 The impact of transducer spot size on edge effect
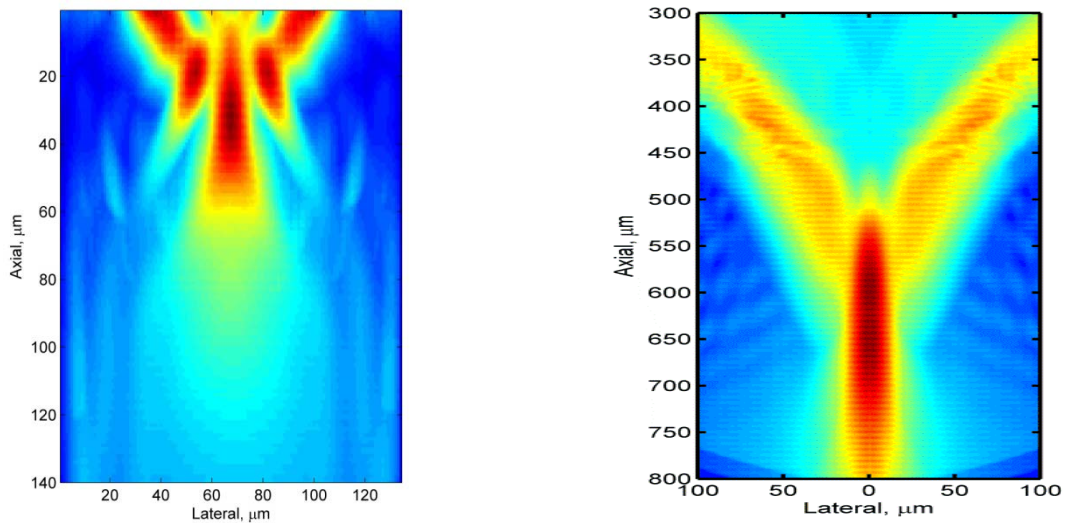
Fig. 12. Acoustic beam profile at various focal points in silicon. (a) 35 µm (b) 700 µm

Fig. 12(a) shows the VT beam profile inside a pure silicon block when replacing the test sample using the silicon block under the configuration of Fig. 3, i.e., the VT is placed 10 µm below the Virtual Transducer. Under such a configuration, the VT is focused at the 35 µm depth position inside the silicon block. From Fig. 12(a), the effective spot size inside the silicon is measured as 19 µm using the -6 dB rule. The "influence region" in the C-Line profile as shown in Fig. 11 is 38 µm which is a doubled spot size when considering both sides of the solder bump. Within this region, the gradient changing in the C-Line plot profile is correlated to the influence region.

The same simulation is repeated with a 900 µm thick silicon block and the VT is calibrated to achieve a focal point at 700 µm. Under this configuration, the VT beam profile inside the silicon is shown in Fig. 12(b). From Fig. 12(b), the spot size in silicon is measured as 34 µm. This shows that the acoustic beam diffuses when penetrating thicker materials. Therefore the influence region in the C-Line profile for the 700 µm silicon die is 68 µm. The edge effect profile from the experimental results shown in Fig. 10 compares favourably with an influence region of 68µm. It is worth nothing that the simulation for 700 µm depth was carried out at lower finite element densities because it is impractical to carry out at high finite element densities using our PC due to the enormity of the model. Imperfections and circuitry in the actual flip chip sample will also diffuse the acoustic beam. Therefore a relative big error is expected.

To obtain a quantitative comparison, we recall that the *dip width* of the model A1 is 12 µm (D_{A1}) which was measured with a spot size of 19 µm (S_{Si}) in silicon. The *dip widths* from the experimentally obtained C-scan images as shown in Fig. 10 are 35 µm (D_{M1}) and 44 µm (D_{M2}) respectively. By a simple extrapolation, the corresponding spot sizes in silicon can be predicted from D_{M1} and D_{M2} as: $\frac{S_{Si}}{D_{A1}} \times D_{M1} = 55$ µm and $\frac{S_{Si}}{D_{A1}} \times D_{M2} = 69$ µm.

In Fig. 12(b), the VT produced a spot size of 34 µm in silicon. But considering the spot size in water for the simulation was 16 µm which is 6.6% bigger than 15 µm of the physical transducer spot size in water. The spot size measurement from the 700 µm silicon block simulation is then adjusted from 34 µm to 36 µm. Comparing to 55 µm, there is still a big difference of the spot sizes between the extrapolated measured and simulated results. This indicates two possibilities: the diffusion of the acoustic beam is greater in physical samples or

the relationship between the *dip width* and the spot size do not scale linearly. The former is likely, since the physical sample contains actual circuits etched into the silicon.

5. Conclusions

An acoustic simulation technique for acoustic micro imaging of flip chip packages has been developed. A C-Line plot technique has been proposed to characterize the edge effect of acoustic C-scan images. Finite element analysis shows that the edge effect in acoustic images of flip chip packages is mainly attributed to the UBM structure. Without the UBM structure, the edge effect can be significantly reduced. Simulation results also show that the position of the transducers focal point and the spot size has a significant impact on the edge effect generation. Slightly off-focusing can reduce the edge effect severity although the image is less clear. Preliminary work to predict in situ spot sizes by analyzing the dip width were inconclusive with further work required.

References

[1] J.E. Semmens. Flip chips and acoustic micro imaging: an overview of past applications, present status, and roadmap for the future. Microelectronics Reliability, 2000. **40**(8–10): p. 1539-1543.

[2] R.S.H Yang, D. R. Braden, G.-M Zhang, and D.M. Harvey. Through Lifetime Monitoring of Solder Joints Using Acoustic Micro Imaging. Soldering and Surface Mount Technology, **24**(1) (2012), p.30-37.

[3] R.S.H Yang, D. R. Braden, G.-M Zhang, and David M. Harvey. An automated ultrasonic inspection approach for flip chip solder joint assessment. Microelectronics Reliability, **52**(12) (2012), p. 2995-3001.

[4] S. Brand, P. Czurratis, P. Hoffrogge b, and M. Petzolda. Automated inspection and classification of flip-chip-contacts using scanning acoustic microscopy. Microelectronics Reliability, **50**(9–11) (2010), p. 1469-1473.

[5] G.-M Zhang, D. M. Harvey, and D.R. Braden. Signal denoising and ultrasonic flaw detection via overcomplete and sparse representations. The Journal of the Acoustical Society of America, 124(5)(2008), pp. 2963-2972.

[6] C. Lee, G.-M. Zhang, and D. M. Harvey. Analysis of solder joint edge effect in acoustic micro imaging of microelectronic packages: a preliminary study. in the 4th Electronic System-Integration Technology Conference (ESTC), 2012, p.1-4.

[7] C. Lee. Numerical study for acoustic micro-Imaging of three dimensional microelectronic packages. PhD thesis, Liverpool John Moores University, 2014.

[8] E. H. Amalu and N. N. Ekere. Prediction of damage and fatigue life of high-temperature flip chip assembly interconnections at operations. Microelectronics Reliability, **52**(11)(2012), p. 2731-2743.

[9] M.J. Varnau. Impact of wafer probe damage on flip chip yields and reliability. in 19th Electronics Manufacturing Technology Symposium, IEEE/CPMT, 1996.

[10] J.E. Semmens and L.W. Kessler. Evaluation of chip scale packaging using acoustic micro imaging: an overview of applications, limitations and directions for future developments. in Pan Pacific Microelectronics Symposium, 1998.

Figure Captions

Fig. 1. Fig. 1. A plan of a c-scan image of flip chip package soldered on a PCB board using a 230 MHz transducer with a spot size of 16 µm and focal depth of 186 µm.

Fig. 2. Typical C-scan images of solder joints extracted from Fig. 1.

Fig. 3. The geometrical model for acoustic simulation (units in µm).

Fig. 4. The virtual transducer derived from the physical transducer to reduce computational load.

Fig. 5. The models A1and A2.

Fig. 6. The model B.

Fig. 7. (a) Simulated B-scan image and (b) comparison with model

Fig. 8. (a) A C-Line plot obtained from the simulated B-scan image in Fig. 7(a); (b) C-scan image created from the C-Line plot of Fig. 8(a).

Fig. 9. (a) A measured C-scan image and (b) two resultant C-Line plots.

Fig. 10. Comparison of measured and simulated C-Line with annotations

Fig. 11. C-Line profile comparison between the models A1, A2 and B for half a solder bump.

Fig. 12. Acoustic beam profile at various focal points in silicon. (a) 35µm (b) 700µm.

Table Captions

Table 1: Three finite element models.

Table 2: Model parameters.

Table 1: Three finite element models.

Model Name	Silica Connection	Additional Parameters
Model A1	UBM	Focal point at centre of UBM sandwich
Model A2	UBM	Focal point in solder bump 3µm below UBM
Model B	NO UBM	Focal point at centre of UBM sandwich

Table 2: Model parameters.

Structure	Parameters
Solder Bump Diameter	140 µm
Solder Material	Tin-Lead (60:40)
UBM Composition	Al, NiV, Cu; Ratio 1:1:1
UBM Thickness	10 µm
Silicon Die Thickness	33 µm